Horizon 2020
European Union funding
for Research & Innovation

Horizon 2020 Grant Agreement Number 734798
indoor small-cell Networks with 3D MIMO Array Antennas
(is3DMIMO)

D1.1

Mechanism of Sub-path Generation in 3D Ray-Launchinng

Authors(s)	Qi Hong, Xi Liao, Yu Shao, Yang Wang, Jiliang Zhang, and Andrés Alayón Glazunov
Author(s) Affiliation	University of Sheffield, UK, Chongqing University of Posts and Telecommunications, P. R. China; Chalmers University of Technology, Sweden; Lanzhou University, P. R. China
Editor(s):	Andrés Alayón Glazunov, and Xiaoli Chu
Status-Version:	Final-1.0
Project Number:	734798
Project Title:	indoor small-cell Networks with 3D MIMO Array Antennas (is3DMIMO)
Project Acronym:	is3DMIMO
Work Package Number	1

Abstract

The millimeter-wave bands, such as 40 GHz-50GHz are promising for use in future 5G wireless networks, especially for serving indoor hot spots. Appropriate indoor channel models are critical to the simulation and the evaluation of indoor millimeter-wave wireless networks. The ray launching (RL) channel models have been widely employed to predict indoor radio channels for system design and evaluation. Many state of the art RL models use specular reflections, which work well in low frequency bands. However, in the millimeter-wave bands, the surface roughness is not negligible because the smaller wavelength size is comparable to the roughness of the surface. In millimeter-wave bands, the reflection could be diffused and the electromagnetic waves are scattered away from the surface in a range of directions. To support the 3D RL channel modeling which takes diffuse reflection into account, we investigate the reflection of millimeter-wave bands by typical building structures through measurements. Firstly, we explain the mechanism of the diffuse reflection in millimeter-wave and describe how to take it into account in RL tools. In a diffuse reflection, the scattering exponent is the most important parameter to model the severity of the diffuse reflection. Then, in order to analyse scattering exponents for various types of building materials, a frequency domain measurement system is produced by using a vector network analyzer. The reflection of 40 GHz-50 GHz millimeter-wave signals caused by typical building structures is practically measured in an open space environment. To separate two adjacent rays, respectively, reflected by the front and the back surfaces of the thin board shaped material, a minimum Euclidean distance estimator is proposed, and validated based on the measurement data. Finally, the scattering exponents are extracted form measurement results. Measurements show that the measured values of scattering exponents varies from 30 to 70 for typical materials of building structures. The measured scattering exponents will be employed in Task 1.2 for 3D SCM MIMO channel modelling and characterisation.

Keywords: Diffuse reflection, Ray launching channel model, Multipath generation, Measurement.

Contents

1   Introduction

The predictable rapid increase of indoor mobile data growth in the future wireless communication leads to a growth in the operating frequency of communication system. Due to most bands in low frequency already allocated, the millimeter-wave bands such as 40 GHz-50 GHz are promising for use in future wireless networks [1]. To thoroughly investigate millimeter-wave, it is critical to have a good understanding of millimeter-wave radio-propagation. Appropriate indoor channel models are also required to simulate and evaluate millimeter-wave wireless networks.

The ray tracing (RT) and the ray launching (RL) channel models are employed to predict the radio channel for system design and evaluation [2–5]. For example in [2], a vertical plane launch technique for approximating a full 3D site specific ray-tracing tool to predict propagation is proposed by the authors. In [3], an RL algorithm is presented to estimate the radio-propagation in a small-cell wireless system. In [4], the RL tool is used to generate the parameters such as signal strength and angle of arrival for all possible paths. In [5], the authors provided a technique based on collaborative filtering to improve the RL tool.

Many state-of-the-art RT and RL models use specular reflections to simulate reflected rays. For each incident ray, the angle of incidence equals the angle of reflection. Meanwhile, the incident, normal, and reflected directions are coplanar following the law of specular reflection. For specular reflections, smooth surface is necessarily assumed. In general, it works well in low frequency bands, e.g., widely used 2.4 GHz and 5.8 GHz. However, in the millimeter-wave bands, the surface roughness can't be neglected because the smaller wavelength size is comparable to the roughness of the surface. The reflection may be diffused and the electromagnetic waves are scattered away from the surface in a range of directions. Therefore, the diffuse reflection effect should be taken into account in millimeter-wave channel modelling.

Recently, diffuse reflection effects were taken into account in RT and RL models [6–11]. In [6], various effective-roughness diffuse scattering models are given and justified by measurement. Different scattering coefficients have also been estimated from measurements. In [9], diffuse scattering from rough surfaces in THz is estimated by using RT tool. In [10], the authors proposed a new method to model the channel in straight tunnels with an arch-shaped cross section, and in curved tunnels with a rectangular cross section by using an RL tool. Recently, in [11], an RL tool is used to simulate a typical urban scenario in the WINNER - II channel model. There, it was shown that the diffuse reflection is higher at 28 GHz than that at low frequencies, e.g., 2.4 GHz. Previous works have analyzed the

impact of diffuse reflection evaluated by RT and RL tools. However, the impact of diffuse reflection on millimeter-wave propagation, especially the 40 GHz-50 GHz band, still not well-understood.

In this deliverable, to support the 3D ray launching channel modeling which takes diffuse reflection into account, we investigate the reflection of millimeter-waves by typical building structures through measurements. More specifically, contributions of this deliverable are as follows. Firstly, we explain the mechanism of the diffuse reflection at millimeter-wave frequencies and describe how to take it into account in RL tools. Then, in order to analyse scattering exponents for various types of building materials, a frequency domain measurement system is produced by using a vector network analyzer. The reflection of 40 GHz-50 GHz millimeter-wave signals caused by typical building structures is practically measured in an open space environment. Third, to separate two adjacent rays, respectively, reflected by the front and the back surfaces of the thin board shaped material, a minimum Euclidean distance estimator is proposed, and validated based on the measurement data. Finally, the scattering exponents are extracted form measurement data.

The remainder of this deliverable is organized as follows. In Section 2, the mechanism of diffuse reflection is given. The reflection ray generation in 3D ray launching is described in Section 3. In Section 4, we setup the experiment and do some measurement under various materials. The simulation results are presented in Section 5. Finally, some conclusions are drawn in Section 6.

2 Diffuse reflection

2.1 Mechanism of diffuse reflection

In the millimeter-wave band, the effect of diffuse reflection has to be considered during channel modeling because the roughness of reflection surface is not negligible compared with the wavelength. Diffuse scattering is the signals scattered to several directions rather than one specular direction, as illustrated in Fig. 1.

For the directive model, it is assumed that the maximum power of the scattering rays is the specular reflection ray. In order to comply with this assumption, the following expression is considered [6]

$$E_s^2 = E_{s0}^2 \left(\frac{1 + \cos(\xi_R)}{2} \right)^{\alpha}, \tag{1}$$
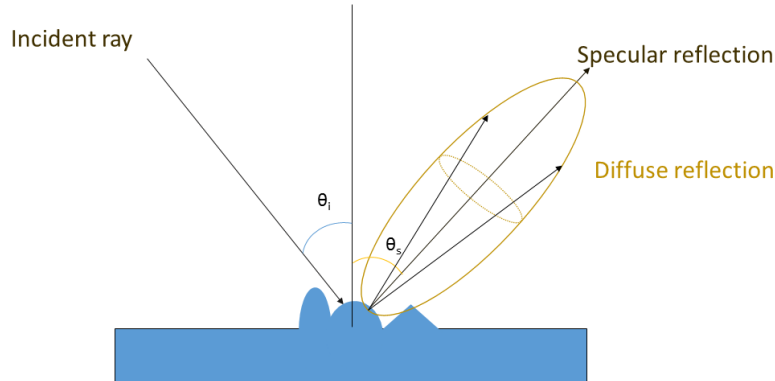
Figure 1: Diffuse reflection.

where E_{s0} is the maximum amplitude of the specular reflection field, ξ_R is the angle between the specular reflection ray and other scattering rays. The scattering exponent α represents the width of the scattering lobe which is an adjustable variable for various materials. The E_{s0} is given by

$$E_{s0} = \left(\frac{KS}{r_i r_s}\right)^2 \frac{\delta_s \cos(\theta_i)}{F_\alpha},\tag{2}$$

$$F_\alpha = \frac{1}{2^\alpha} \sum_{\eta=0}^{\alpha} \binom{\alpha}{\eta} I_\eta,\tag{3}$$

,

$$I_\eta = \frac{2\pi}{\eta+1}\left[\cos(\theta_i)\sum_{\beta=0}^{\frac{\eta-1}{2}} \binom{2\beta}{\beta}\frac{\sin^{2\beta}(\theta_\eta)}{2^{2\beta}}\right]^{\left(\frac{1-(-1)^\eta}{2}\right)}.\tag{4}$$

From (4), the power of the diffuse reflection is mainly determined by the specular reflection field, the scattering angle and the scattering exponent α which is the scattering lobe. Therefore, we focus on the investigation of α.

2.2 Two-ray model for thin board reflection

For thin boards, we need to consider the resonant phenomenon caused by multiple reflections and transmissions as shown in Fig. 2. As can be seen, the reflected electromagnetic waves are comprised by the direct reflection ray (named the first ray in the remainder of
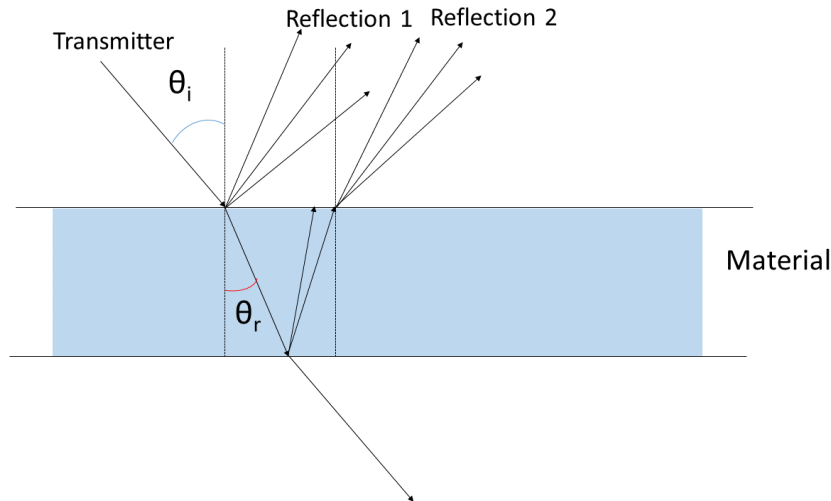
Figure 2: Multiple reflections and transmissions.

this deliverable) and the reflection ray (the second ray) from the back side of the thin board. In the analysis of the diffuse reflection from the material surface, the first ray is the contribution to the diffuse reflection that we want to study, while the second ray is considered as interference. Below we present the mathematical model for our analysis.

Firstly, the measured S_{21} is the composition of both rays and other multipaths in the measurement environment.

$$
\begin{aligned}
S_{21}(\omega) &= \Gamma_1(\omega)\exp(jkr_1) + \Gamma_2(\omega)\exp\{j[k(r_1+\Delta r)+\phi]\} + S_m \\
&= \Gamma_1(\omega)\exp(j\omega r_1/c) + \Gamma_2(\omega)\exp\{j[\omega(r_1+\Delta r)/c+\phi]\} + S_m,
\end{aligned}
\tag{5}
$$

where r_1 and r_2 are the path lengths of the first and the second rays, $\Gamma_1(\omega)\exp(j\omega r_1/c)$ is the amplitude of the single reflection ray and $\Gamma_2(\omega)\exp[j(\omega(r_1+\Delta r)/c+\phi)]$ is the amplitude of the second reflection ray, ϕ is the phase shift relative to the first ray, $c = 3 \times 10^8$ m/s is the speed of light. $\Gamma_1(\omega)$ and $\Gamma_2(\omega)$ are the amplitudes of the first and the second rays at the surface of the material, respectively, whereas Δr is the difference of the two path lengths. According to the Friis transmission formula, the amplitude of $\Gamma_1(\omega)$ and $\Gamma_1(\omega)$ are inversely proportional to ω, and therefore, we assume that $|\Gamma_1| = \gamma_1/\omega, |\Gamma_2| = \gamma_2/\omega$, where γ_1 and γ_2 are two scaling factors. Without loss of generality, $\gamma_1 > \gamma_2$. $S_m \sim \mathcal{CN}(0,\sigma_m^2)$ denotes the combined S_{21} of multipaths except the first and the second rays. Because the first and the second rays, are the dominant reflect rays in the measured S_{21}, it can be assumed that the combined effect of the higher order behave like white noise where $\sigma_m^2 << |\Gamma_i|^2, i = 1, 2$.

It should be noted that the final results of the reflection rays are determined by properties of both rays. However, resolving the contribution of each multipath component
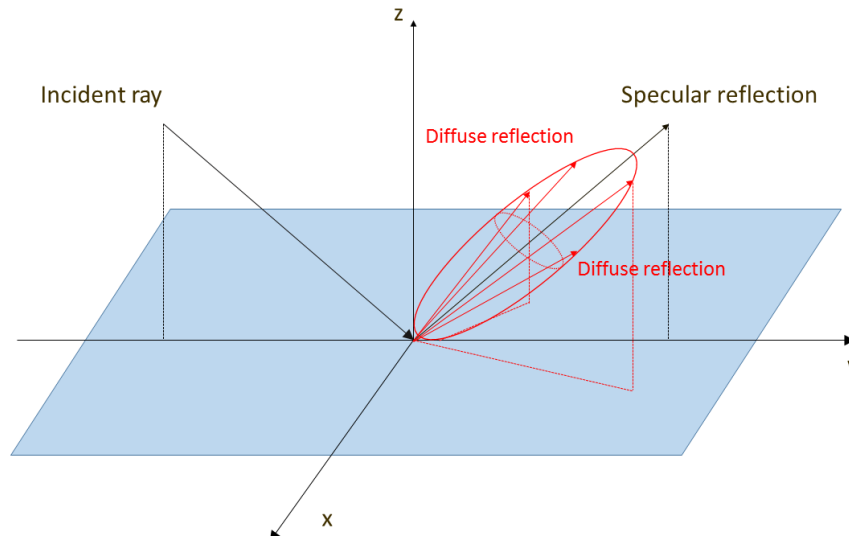
Figure 3: 3D diffuse reflection.

in (5) is challenging because the first and second rays arrive very closely at the surface of the thin board, and the spatial resolution is not sufficiently good to distinguish them. In the measurement section, an algorithm to resolve them is proposed.

3   Reflection ray generation in 3D ray launching

The purpose of this subsection is to discuss issues concerning implementation of the reflection ray generation in 3D RL channel model while diffuse reflection is taken into account. In an RL channel model, the rays are computed from the transmitter. Basically, while the ray hits the blockage building structure, a specular reflection ray is generated. However, taking diffuse reflection into account, multiple rays are generated at the reflection point on the surface.

Due to the roughness of the reflecting surface, the diffuse reflection rays will extend into different directions as shown in Fig. 3. In 3D space, the scattering exponent α, which is named as 'scattering width', determine the scattering lobe which mainly affects the angle-of-arrival/departure in millimeter-wave channel model [6]. The 3D diffuse reflection rays can be generated in the RL tools if the frequency dependence of α is empirically is empirically modeled through measurements.

First, let's assume n scatter rays are generated in one reflection, then, parameters in (1), i.e., α and E_{s0} are generated through measurement-based empirical models. Second, the reflection point is considered as a transmit antenna and create an array of $n-1$

Table 1: Size of studied materials.

Materials	length (cm)	width (cm)	thickness (cm)
Wooden board	121.5	80.7	1.7
Plaster board	119.8	79.0	0.9
Granite	121.5	80.7	1.7

independent and identically distributed (i.i.d.) random scatter rays, with a power azimuth spectrum given by (1). Third, the n generated rays are emitted to continue the simulation of the RL model.

4   Measurement

In order to investigate the diffuse reflection, especially the scattering exponent α in (1), we establish a measurement system and measure the diffuse reflection parameters for typical materials of building structures. In this section, the measurement set-up is introduced.

4.1   Equipment and materials

In this section, a Vector network analyzer (VNA) based measurement system is described. In the system, the VNA is employed to measure the $S_{21}(\vec{\omega})$ of the transmission channel via reflection from the analysed materials, where the measurement is carried out at 40 GHz-50 GHz and $\vec{\omega} \triangleq [40, 40.25, 40.5, ..., 49.75, 50]$ GHz. Two horn directional antennas with high gains are connected to the VNA via cables to transmit and receive radio frequency signals. the cables have a loss of 20 dB at 45 GHz. The VNA plus cables are calibrated by short, open, load and through (SOLT) standards. With a high directionality, the antennas effectively reduce the interference from unwanted directions efficiently. A laptop is used to collect and analyse the data from the VNA.

   In this work, typical materials of building structures, i.e., wooden board, plaster board and granite, are measured. A photo of the measurement samples are illustrated in Fig. 4, and their size are shown in Table 1. The thickness of the measured material is no larger than 2 cm, and therefore, the two ray model has to be considered.

Woodenboard   Plasterboard   Granite
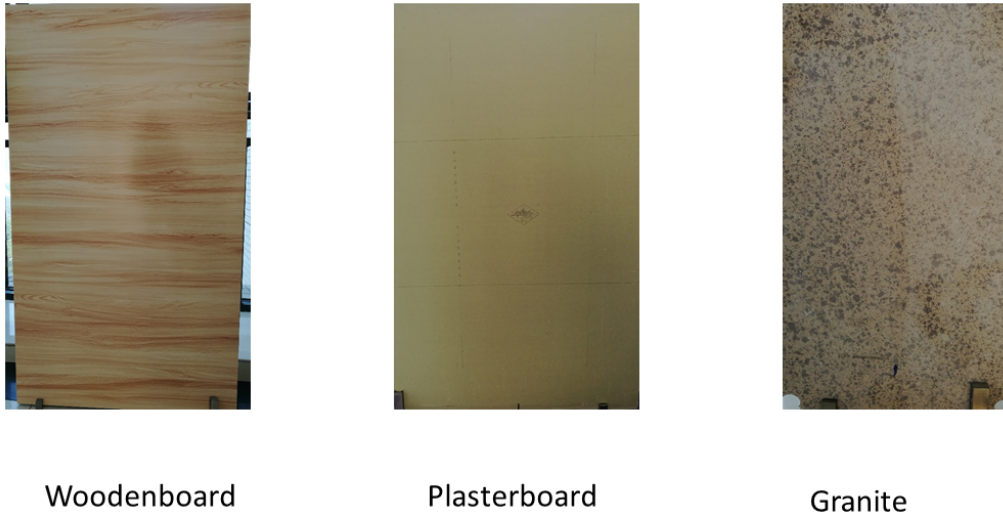
Figure 4: Measured materials.

Figure 5: Measurement set-up.
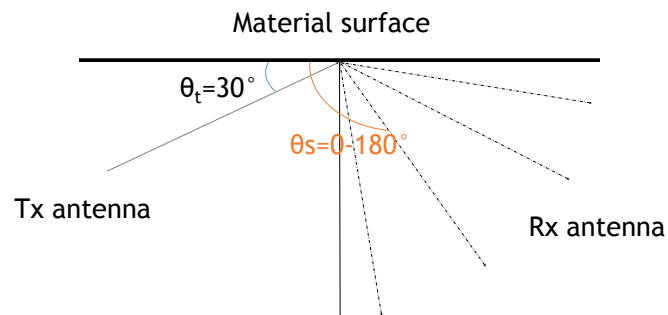
Figure 6: Illustration of the reflected signal measurement procedure.
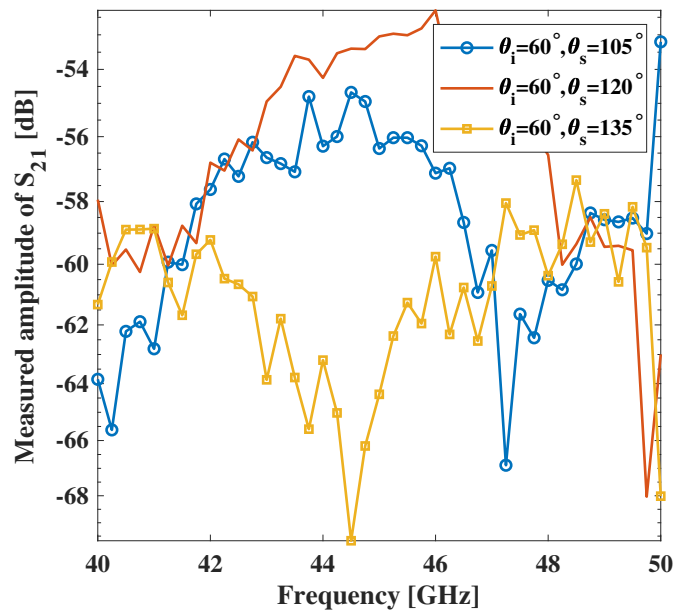
Figure 7: Example of the magnitude of measured S_{21} via wooden board reflection. The incident angle is 60°.
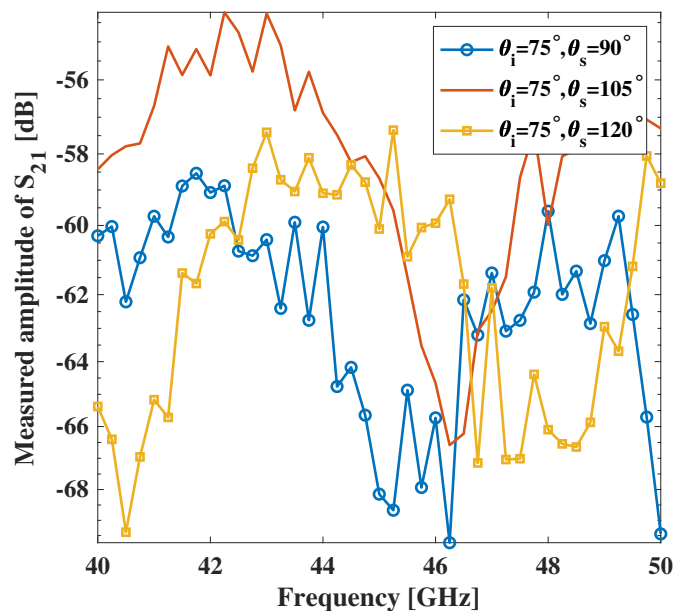
Figure 8: Example of the magnitude of measured S_{21} via wooden board reflection. The incident angle is 75°.

4.2 Measurement procedure

A scheme of the measurement set-up is shown in Fig. 5. During each measurement, the antennas are mounted on tripods and kept at fixed locations to ensure consistent measurement conditions for all the construction materials. Meanwhile, the height and polarization of the antenna can be adjusted. For each material, we carry out the measurement at 40 GHz-50 GHz bands with interval 250 MHz. The angle of Tx antenna are $60°, 75°$ as illustrated in Fig. 6. The position of the Rx antenna is located at $15°$ away from both sides of the specular reflection angle. Considering 10λ distance as the boundary of the far field, the far field boundary of 40 GHz-50 GHz band is 6.5 cm-7 cm. In order to satisfy the far-field condition, the distance between the antennas and the scattering position is 50 cm, which leads to a path loss.

Examples of the absolute value of the measured S_{21} parameters are given in Figs. 7-8, where the incident angles are $60°$ and $75°$, respectively. To estimate scattering exponents from measurements, we need the properties of the first reflection ray. However, Figs. 7-8 show that the measured S_{21} is superimposition of multiple rays including the first ray and the second ray in Fig. 2, as well as the multipath in the measurement environment. In the next subsection, how to extract the properties of the first ray from the measured S_{21} is addressed.

4.3 Reflection rays resolution

The two-ray propagation mechanism makes challenges on measurement data processing if the materials are in shapes of thin board. In a practical measurement set-up, the resolution of the two rays is not straightforward. For example, even if the measurement bandwidth is as large as 10 GHz, the resolution of Δr is 3 cm only, which is comparable to the thickness of the involved material. It is difficult to distinguish them in the time domain, because of the side lobe introduced by IFFT with rectangular window in the frequency domain. To address this problem, an algorithm to separate the referred two rays is given as follows.

First, the receive power obtained from the $S_{21}(\omega)$ as a result of the superimposition of the first and the second rays is computed by

$$
\begin{aligned}
|S_{21}(\omega)|^2 &= |\Gamma_1(\omega) + \Gamma_2(\omega)\exp[j(\omega\Delta r/c + \phi)]|^2 \\
&= |\Gamma_1(\omega)|^2 + |\Gamma_2(\omega)|^2 + 2|\Gamma_1(\omega)||\Gamma_2(\omega)|\cos(\omega\Delta r/c + \phi) + P_m/\omega^2,
\end{aligned}
\tag{6}
$$

where P_m/ω^2 is the error introduced by multipath.

Therefore, by multiplying ω^2 on both sides of the above expression, we have

$$|S_{21}(\omega)|^2\omega^2 = \gamma_1^2 + \gamma_2^2 + 2\gamma_1\gamma_2\cos(\omega\Delta r/c + \phi) + P_m. \tag{7}$$

In order to extract γ_1 from the measured $S_{21}(\vec{\omega})$, we propose a minimum least squares method (MLSM) inspired by (7). The basic mechanism of MLSM is to minimize the mean square distance between the measured and the estimated S_{21} parameters, i.e.

$$
\begin{aligned}
[\hat{\gamma}_1, \hat{\gamma}_2, \Delta\hat{r}, \hat{\phi}] &= \arg\min \left\|\hat{\gamma}_1^2 + \hat{\gamma}_2^2 + 2\hat{\gamma}_1\hat{\gamma}_2\cos(\vec{\omega}\Delta\hat{r}/c + \hat{\phi}) - |S_{21}(\vec{\omega})|^2\vec{\omega}^2\right\|^2 \\
&= \arg\min \left\{ (\hat{\gamma}_1^2 + \hat{\gamma}_2^2)^2 + \|2\hat{\gamma}_1\hat{\gamma}_2\cos(\vec{\omega}\Delta\hat{r}/c + \hat{\phi})\|^2 + \||S_{21}(\vec{\omega})|^2\vec{\omega}^2\|^2 \right.\\
&\quad + \text{MEAN}_\omega[2(\hat{\gamma}_1^2 + \hat{\gamma}_2^2)(2\hat{\gamma}_1\hat{\gamma}_2\cos(\omega_i\Delta\hat{r}/c + \hat{\phi}))] \\
&\quad - \text{MEAN}_\omega[2(2\hat{\gamma}_1\hat{\gamma}_2\cos(\omega_i\Delta\hat{r}/c + \hat{\phi}))(|S_{21}(\omega_i)|^2\omega_i^2)] \\
&\quad \left. - \text{MEAN}_\omega[2(\hat{\gamma}_1^2 + \hat{\gamma}_2^2)(|S_{21}(\omega_i)|^2\omega_i^2)] \right\},
\end{aligned}
\tag{8}
$$

where $[\hat{\gamma}_1, \hat{\gamma}_2, \Delta\hat{r}, \hat{\phi}]$ are unknown parameters that are independent of frequency, $\|\vec{a}\|^2 \triangleq \sum_{i=1}^{N} |a_i|^2$ is a norm for a vector $\vec{a} \triangleq [a_1, a_2, ..., a_N]$, $\text{MEAN}_\omega[.] \triangleq \frac{1}{41}\sum_{i=1}^{41}[.]$ is the sample mean operation over all elements of $\vec{\omega}$, and $\omega_i, i = 1, 2, ..., 41$ denotes the i-th element of $\vec{\omega}$. Using exhaustive searching by (8) to jointly estimate $[\hat{\gamma}_1, \hat{\gamma}_2, \Delta\hat{r}, \hat{\phi}]$ is computational expensive. To reduce the computational complexity, we estimate the $[\hat{\gamma}_1, \hat{\gamma}_2]$ and $[\Delta\hat{r}, \hat{\phi}]$, separately.

Step 1: We will estimate the $[\Delta\hat{r}, \hat{\phi}]$ first. Since

$$\text{MEAN}_\omega\left[2\hat{\gamma}_1\hat{\gamma}_2\cos(\omega_i\Delta\hat{r}/c + \hat{\phi})\right] \approx \text{MEAN}_\omega\left[2\gamma_1\gamma_2\cos(\omega_i\Delta r/c + \phi)\right] \approx 0, \tag{9}$$

and

$$\text{MEAN}_\omega[\cos^2(\omega_i\Delta\hat{r}/c + \hat{\phi})] \approx \text{MEAN}_\omega[\cos^2(\omega_i\Delta r/c + \phi)] \approx 0.5, \tag{10}$$

Substituting (9) and (10) into (8), we have

$$
\begin{aligned}
[\hat{\gamma}_1, \hat{\gamma}_2, \Delta\hat{r}, \hat{\phi}] &= \arg\min \left\{ (\hat{\gamma}_1^2 + \hat{\gamma}_2^2)^2 + 2\|\hat{\gamma}_1\hat{\gamma}_2\|^2 + \||S_{21}(\vec{\omega})|^2\vec{\omega}^2\|^2 \right.\\
&\quad - 4\hat{\gamma}_1\hat{\gamma}_2\text{MEAN}_\omega[\cos(\omega_i\Delta\hat{r}/c + \hat{\phi})|S_{21}(\omega_i)|^2\vec{\omega}^2] \\
&\quad \left. - 2\text{MEAN}_\omega[(\hat{\gamma}_1^2 + \hat{\gamma}_2^2)|S_{21}(\omega_i)|^2\omega_i^2] \right\}.
\end{aligned}
\tag{11}
$$

From (11), for any given $\hat{\gamma}_1$ and $\hat{\gamma}_2$, we have

$$[\Delta\hat{r}, \hat{\phi}] = \arg\max \left\{ \text{MEAN}_\omega\left[|S_{21}(\omega_i)|^2\omega_i^2\cos(\omega_i\Delta\hat{r}/c + \hat{\phi})\right] \right\}. \tag{12}$$

After measurement, the estimators of $[\Delta\hat{r}, \hat{\phi}]$ is obtained by exhaustively search.

Step 2: After substituting the $[\Delta\hat{r}, \hat{\phi}]$ into the equation (8), the $[\hat{\gamma}_1, \hat{\gamma}_2]$ is estimated through the MLSM principle as

$$[\hat{\gamma}_1, \hat{\gamma}_2] = \arg\min \left\| \hat{\gamma}_1^2 + \hat{\gamma}_2^2 + 2\hat{\gamma}_1\hat{\gamma}_2 \cos(\vec{\omega}\Delta\hat{r}/c + \hat{\phi}) - |S_{21}(\vec{\omega})|^2\vec{\omega}^2 \right\|^2 \qquad (13)$$

Examples of two rays resolution are considered in Figs. 9-11. The incident angle is 60° and the reflection angle is 120°. It is observed that the combination of the separated rays matches the measured S_{21} parameter very well, and the resolution is validated. In the following analysis, the first ray for every reflection angle is evaluated as the reflection signal.
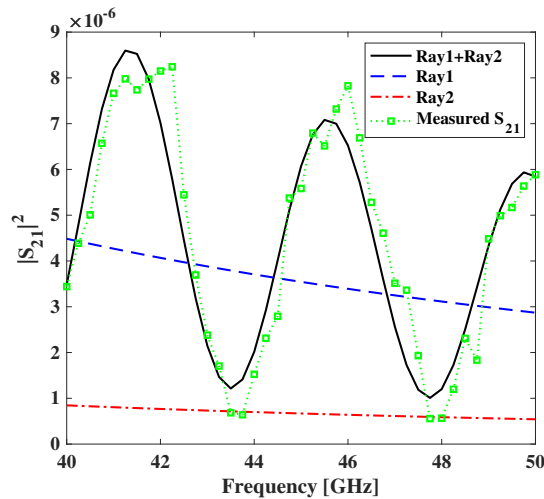
Figure 9: Example of two ray resolution for granite with an incident angle of 60° and a reflection angle of 120°.

5 Measurement results

5.1 Parameter estimation

In this subsection, the scattering exponent α in the diffuse reflection model is estimated through measured data. After resolution of multiple rays, the S_{21} of the first ray is obtained as

$$S_{21}(\omega) = \frac{\hat{\gamma}_1}{\omega} \exp(j\omega r_1/c). \qquad (14)$$
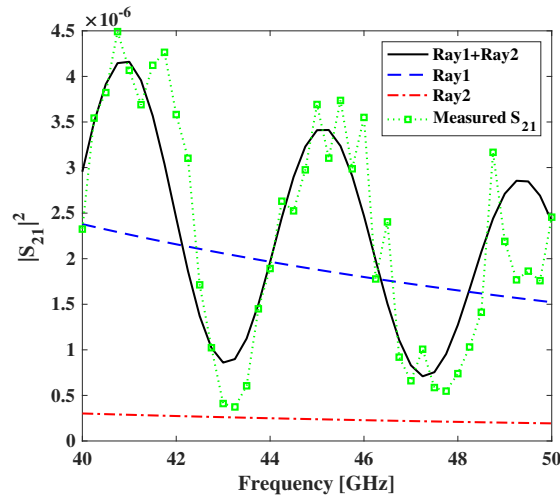
Figure 10: Example of two ray resolution for granite with an incident angle of 60° and a reflection angle of 105°.
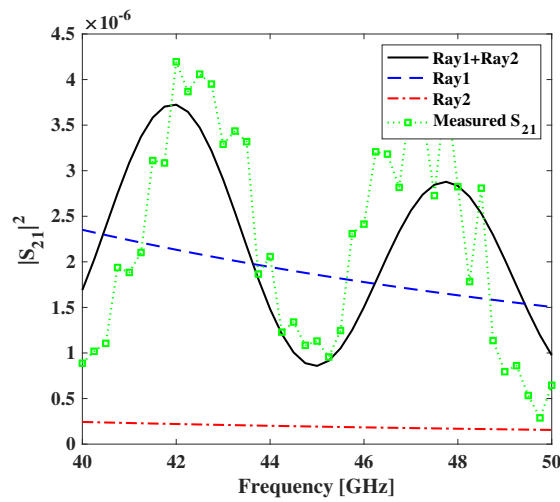
Figure 11: Example of two ray resolution for granite with an incident angle of 60° and a reflection angle of 135°.

Therefore, substituting equation (14) into (1), we obtain

$$\left(\frac{\gamma_1(\xi_R)}{\omega}\right)^2 = L^{-1}(\omega)E_{s0}^2 \left(\frac{1 + \cos(\xi_R)}{2}\right)^\alpha. \tag{15}$$

Because the distance between both antennas and the scattering position at the surface of the material is 50 cm in our measurements, we have a path loss on the measurement signal. Using $L(\omega)$ to denote the pathloss with a distance of 1 m and the antenna gains, when $\xi_R = 0$, we have

$$\gamma_1^2(0) = \frac{\omega^2 E_{s0}^2}{L(\omega)}. \tag{16}$$

Therefore, we have

$$\gamma_1^2(\xi_R) = \gamma_1^2(0) \left(\frac{1 + \cos(\xi_R)}{2} \right)^\alpha . \tag{17}$$

Finally, taking logarithm at both sides of (17),

$$\alpha = \frac{2 \ln \left(\frac{\gamma_1(\xi_R)}{\gamma_1(0)} \right)}{\ln \left(\frac{1+\cos(\xi_R)}{2} \right)}, \tag{18}$$

and therefore the estimator of the scattering exponent α is

$$\hat{\alpha} = \frac{2 \ln \left(\frac{\hat{\gamma}_1(\xi_R)}{\hat{\gamma}_1(0)} \right)}{\ln \left(\frac{1+\cos(\xi_R)}{2} \right)}. \tag{19}$$

5.2   Results

Table 2: Measured α under various materials

Material	Incident 60°		Incident 75°	
	$-15°$	$+15°$	$-15°$	$+15°$
Plaster board	35.6	36.7	44.8	31.1
Wooden board	23.8	67.4	54.6	44.3
Granite	37.1	37.3	62.0	37.3

For granite, wooden and plaster board materials, the relationship between the measured α and the incident angle is shown in Table 2. Therein, $-15°$ and $15°$ represent the scattering angles away from both sides of the specular reflection angle. It is found that the measured α varies from 30 to 70, which is larger than that used in [6, 13] because of smoother surfaces of the measured materials. In the future, materials with rough surfaces will be measured.

The contributions in this deliverable have addressed the requirement of Task 1.1 in the is3DMIMO project. In the future, more materials will be involved and a database of α will be established to support Task 1.2. Based on results in this deliverable, a paper draft entitled "Measurement analysis of scattering exponents for typical building materials", targeting IET Electronics Letters, is under preparation by the authors of this deliverable.

6   Conclusion

In this deliverable, the mechanism of the diffuse reflection is described and the reflection ray generation in 3D RL is given. To analyse scattering exponents for various types of

building materials, a frequency domain measurement system is established by using a vector network analyzer. The reflection of 40 GHz-50 GHz millimeter-wave signals caused by typical building structures is practically measured in an open space environment. To separate the referred two rays from measurement data, we proposed an MLSM based algorithm, based on which some measurements are executed to obtain the diffuse properties, especially scattering exponents of typical materials of buildings structures. Measurements show that the measured values of scattering exponents varies from 30 to 70 for typical materials of building structures. The measured scattering exponents will be employed in Task 1.2 for 3D SCM MIMO channel modelling and characterisation.

References

[1] T. S. Rappaport, et. al.,"Millimeter wave mobile communications for 5G cellular: it will work!," *IEEE Access.*, vol. 1, pp. 335-349, 2013.

[2] G. Liang and H. L. Bertoni,"A new approach to 3D ray tracing for propagation prediction in cities," *IEEE Trans. Ant. Pro.*, vol. 46, pp. 853-863, 1998.

[3] M. C. Lawton and J. P. McGeehan,"The application of a deterministic ray launching algorithm for the prediction of radio channel characteristics in small-cell environments," *IEEE Trans. Veh. Technol.*, vol. 43, pp. 955-969, 1994.

[4] Z. Dai, et. al.,"UAV-aided source localization in urban environments based on ray launching simulation," *IEEE USNC/URSI*, pp. 595-596, 2017.

[5] F. Casino, et. al.,"Optimized wireless channel characterization in large complex environments by hybrid ray launching-collaborative filtering approach," *IEEE Trans. Ant. Pro.*, vol. 16, pp. 780-783, 2017.

[6] V. Degli-Esposti, et al.,"Measurement and modelling of scattering from buildings," *IEEE Trans. Ant. Pro.*, vol. 55, pp. 143-153, 2007.

[7] V. Degli-Esposti and H. L. Bertoni,"Evaluation of the role of diffuse scattering in urban microcellular propagation," *IEEE VTC*, 1999.

[8] V. Degli-Esposti, et. al.,"A diffuse scattering model for urban propagation prediction," *IEEE Trans. Ant. Pro.*, vol. 49, pp. 1111-113, 2001.

[9] C. Jansen, et. al.,"Diffuse Scattering From Rough Surfaces in THz Communication Channels," *IEEE Trans. Terahertz Science and Tech.*, vol. 1, pp. 462-472, 2011.

[10] E. Masson, et. al.,"Radio wave propagation in curved rectangular tunnels at 5.8 GHz for metro applications," *EURASIP Journal on Wireless Communications and Networking*, pp. 81-85, 2011.

[11] D. Solomitckii, et. al.,"Characterizing the impact of diffuse scattering in urban millimeter-wave deployments," *IEEE Wire. Commun. Lett.*, vol. 5, pp. 432-435, 2016.

[12] R. Hoppe, et al.,"Accelerated ray optical propagation modelling for the planning of wireless communication networks," *IEEE Raido and Wirelss Conference*, 1999.

[13] J. P. Garcia, et al., "On the importance of diffuse scattering model parameterization in indoor wireless channels at mm-wave frequencies," *IEEE Access*, vol. 4, pp. 688-701, 2016.